ISSN 1063-7745, Crystallography Reports, 2007, Vol. 52, No. 6, pp. 1006–1013. © Pleiades Publishing, Inc., 2007.
Original Russian Text © A.P. Menushenkov, Ya.V. Rakshun, 2007, published in Kristallografiya, 2007, Vol. 52, No. 6, pp. 1042–1050.

QUASICRYSTALS

EXAFS Spectroscopy of Quasicrystals

A. P. Menushenkov[a] and Ya. V. Rakshun[b]

[a] *Moscow Engineering Physics Institute, Kashirskoe sh. 31, Moscow, 115409 Russia*
e-mail: menushen@htsc.mephi.ru

[b] *Budker Institute of Nuclear Physics, Siberian Branch, Russian Academy of Sciences, Novosibirsk, 630090 Russia*

Received March 29, 2007

Abstract—The results of the investigation of the features of the local structure of quasicrystalline materials by extended X-ray absorption fine structure (EXAFS) spectroscopy with the use of synchrotron radiation are analyzed. The advantages of this method from the point of view of deriving information about the local shifts of the atoms forming an icosahedral structure are demonstrated. The rearrangement of the local environment of copper and iron in Al–Fe–Cu ternary alloys at a transition from the crystalline to the quasicrystalline phase has been investigated. It is established that the nearest copper coordination retains the symmetry characteristic of the crystal; however, rotation and small displacements of copper matrix atoms lead to significant rearrangement of aluminum atoms around iron atoms. As a result, icosahedral clusters with pentagonal symmetry are formed around iron atoms and violation of the translational symmetry is accompanied by the transition of Al–Fe–Cu to the quasicrystalline state.

PACS numbers: 61.10.Ht, 61.44.Br

DOI: 10.1134/S1063774507060120

INTRODUCTION

Thermodynamically stable quasicrystals exist in the form of both ternary (Al–Pd–Mn, Al–Cu–Fe, Al–Cu–Ru, etc.) and binary (ZrPd, ZrPt, ZrBe, etc.) alloys. With respect to the degree and character of ordering, they occupy a position between amorphous and crystalline materials: in the absence of translational symmetry, they retain the long-range order in the spatial arrangement of atoms [1]. Owing to the unique strength and tribological properties, quasicrystals can be used as additives and coatings, which do not change the composition of an article but significantly increase the wear resistance, corrosion durability, and mechanical strength of its surface. Although all components of quasicrystals are good metals, the electron density of states at the Fermi level has a singularity of the pseudogap type, and the resistivity of the quasicrystalline phase exceeds by more than an order of magnitude the resistance of alloys both in the crystalline and amorphous states owing to the localization of electrons in stable atomic configurations (clusters) that are deep potential wells (traps) for valence electrons [2].

The symmetry of clusters (in particular, pentagonal) significantly differs from that of the initial crystal structure, a fact indicative of the formation of a new short-range order [3]. The processes of local ordering of atoms upon transition from the crystalline to the quasicrystalline state have not been completely studied. This circumstance is primarily related to the weak sensitivity of the "integral" methods (X-ray diffraction and neutron scattering) to features of local structure. In this study, we demonstrate the advantages of X-ray absorption spectroscopy for studying the local structural ordering in quasicrystals via joint analysis of the extended and near-edge fine structure of the X-ray absorption spectrum of quasicrystalline systems based on Al–Cu–Fe ternary alloys. Combination of the two noted methods makes it possible not only to determine the coordination numbers, distances, and type of atoms in the nearest coordination of copper and iron in quasicrystals but also to refine the character (symmetry) of their mutual arrangement.

EXPERIMENTAL

As a basic method for studying the local crystalline and local electronic structures of quasicrystalline compounds, we chose X-ray absorption spectroscopy with application of synchrotron radiation. This technique is based on two locally sensitive methods: extended X-ray absorption fine structure (EXAFS) spectroscopy and X-ray absorption near-edge structure (XANES) spectroscopy, which are based on the analysis the fine structure arising in X-ray absorption spectra above the absorption edge of an individual element entering the composition of a complex compound.

It is agreed that the XANES region extends by 50–100 eV beyond the absorption edge and is determined by the local density of free states of an absorbing atom and the contribution from scattering of an excited photoelectron from the potentials of several atoms of the coordination (the multiple-scattering effect). This process depends on the sufficiently large mean free path of the photoelectrons excited with small wave vectors.

The fine structure observed in the energy dependence of the absorption cross section of X-ray photons whose energies exceed by 100–1500 eV the ionization threshold of the core atomic level under consideration was referred to as the extended fine structure: EXAFS. In contrast to XANES, this structure is mainly due to the single scattering of a photoelectron from the potentials of neighboring atoms. The boundary between these regions is fairly arbitrary and is determined by the magnitude of the photoelectron wave vector at the boundary of the first Brillouin zone: $k_D = 2\pi/d$, where d is the lattice parameter. However, EXAFS spectra are sensitive only to the type of the atoms surrounding an absorbing ion and to the distance between them, whereas XANES spectra are sensitive to changes in the local symmetry of the atomic arrangement.

The physical cause of the fine oscillating structure is the interference of the primary photoelectron wave with the secondary waves formed upon scattering from the surrounding atoms. An analytical formula for the absorption coefficient in the single-scattering region (EXAFS) can be obtained in the semiclassical approximation; i.e., when an X-ray photon is replaced with an electromagnetic wave field. In this case, the photoelectron formed as a result of ionization of an atomic core level is described within the quantum-mechanical approximation.

The experimentally measured absorption coefficient in a sample of thickness x has the form

$$\mu = -(1/x)\ln(I_t/I_0), \quad (1)$$

where I_t is the X-ray intensity transmitted through the sample and I_0 is the intensity of incident X rays.

The oscillating part $\chi(k)$ of the absorption coefficient, referred to as the EXAFS function, is determined from the relation

$$\chi(k) = \frac{\mu(k) - \mu_0(k)}{\mu_0(k)}. \quad (2)$$

Here, $\mu(k)$ is the experimental absorption coefficient, $\mu_0(k)$ is a gradually varying function describing the so-called absorption coefficient of a "free atom," and k is the photoelectron wave vector:

$$k = \sqrt{2m_e(E - E_0)}/\hbar, \quad (3)$$

where m_e is the electron mass, $\hbar$ is Planck's constant, E is the energy of incident X rays, and E_0 is the energy of the absorption edge under consideration.

For the K-absorption edge, in the plane-wave single-scattering approximation and in the case of harmonic atomic vibrations, the EXAFS function $\chi(k)$ is described by the formula

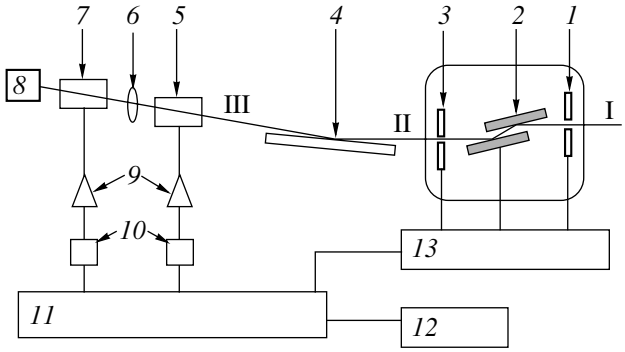

Fig. 1. Schematic diagram of the EXAFS station: (*1*) input collimator, (*2*) monochromator unit, (*3*) output collimator, (*4*) planar X-ray mirror, (*5*) flight ionization chamber monitor (I_0), (*6*) sample (location under the cryostat), (*7*) total-absorption ionization chamber (I_t), (*8*) sandwich trap, (*9*) current-to-voltage converter amplifiers, (*10*) integrating voltmeters, (*11*) crate CAMAC with a microcomputer and necessary modules, (*12*) operating stations, and (*13*) control units for the stepper motors of the monochromator and collimators; (I) white (nonmonochromatic) and (II, III) monochromatic synchrotron radiation beams.

$$\chi(k) = -S_0^2 \sum_n \frac{1}{kR_n^2} N_n |f_n(\pi, k)| \times \exp(-2k^2\sigma_n^2)\sin(2kR_n + 2\delta_l(k) + \phi_n(\pi, k)). \quad (4)$$

Here, summation is performed over all coordination spheres, N_n is the coordination number, R_n is the mean radius of the nth coordination sphere, $f_n(\pi, k)$ is the amplitude of backward scattering of a photoelectron with a wave vector k from atoms of the nth coordination sphere, and σ_n^2 is the mean-square deviation of the interatomic distance from its mean (this deviation is referred to as the Debye–Waller factor). The scale factor S_0^2 takes into account the influence of many-electron effects. The phase shift of the secondary wave is the sum of the geometric phase shift $2kR_n$, which arises on its way to the nth atom and vice versa; the phase $2\delta_l(k)$, gained by an electron with an orbital momentum l during its propagation in the potential of an excited atom; and the phase shift $\phi_n(\pi, k)$, which is caused by backscattering from the nth atom. The amplitudes $f_n(\pi, k)$ and backscattering phases $2\delta_l(\pi, k) + \phi_n(\pi, k)$ are calculated within the quantum-mechanical approximation.

To record XAFS spectra, we used the EXAFS spectrometers mounted in the extraction channel for the synchrotron radiation beam in the VEPP-3 storage ring at the Budker Institute of Nuclear Physics, Siberian Division of the Russian Academy of Sciences (Novosibirsk) and at HASYLAB station E4 (DESY, Hamburg, Germany).

Figure 1 shows a schematic diagram of the EXAFS station E4. The station includes a spectrometer and electronic equipment necessary to automate the spectrometer operation. The spectrometer consists of the following main parts: input and output collimators *1* and *3*, double-crystal monochromator *2*, planar X-ray mirror *4*, and two ionization chambers *5* and *7*. The spectrometer is automated on the basis of a personal computer and electronic equipment in the CAMAC standard.

The monochromator is designed according to the double-crystal scheme, in which the output monochromatic beam is parallel to the input white synchrotron radiation beam and is somewhat displaced in the vertical direction. In this scheme, the wavelength of the monochromatic radiation changes owing to the change in the angle of incidence of the synchrotron radiation beam on the reflecting planes of Si(111) or Si(311) single crystals (Bragg diffraction). The higher harmonics of the radiation are rejected using plane mirrors *4* with a gold coating, which are mounted at the angle of total external reflection for the main harmonic.

Recording of a spectrum implies obtainment of count statistics in gas ionization chambers over a specified time (the typical collection time is about 1 s per point). Energy scanning is performed via rotation of the monochromator crystal by a stepper motor. Since processing of spectra requires passage to an equidistant grid in the k space, the energy step can be set with a quadratic increase, thus increasing the time of count in the far spectral region, where the fine-structure amplitude is small. Under such conditions, the recording time of a fairly extended spectrum ranges from 20 to 40 min.

The Si(111) monochromator of the E4 station provides energy resolutions of ~1.2 and ~1.0 eV in the regions of *K*-Cu- and *K*-Fe-absorption edges, respectively. Low-temperature measurements were performed with a pumped liquid-helium cryostat. The temperature was maintained at a specified level with an error of ~1 K.

Methods of Analysis of EXAFS Spectra

In this study, the EXAFS spectra were analyzed using the VIPER [4] and Ifeffit [5] software packages and the FEFF program [6] for calculating amplitudes and phases.

After calculation of the absorption coefficient from formula (1) and extraction of the EXAFS function (the criterion for correctness is the absence of nonphysical peaks in the Fourier transforms at small R), the isolated signal is subjected to Fourier filtration in specified intervals of the k and R spaces in order to separate the contribution of individual coordination spheres. The windows used (Hanning windows in our case) make it possible to exclude (by smoothing) spurious oscillations related to the limited length of the spectrum. In this case, the function is additionally multiplied by k^2 to increase the signal at large k, expand the spectral region under study, and separate the contributions of light and heavy elements.

The Fourier transform of a signal is not exactly the atomic radial distribution function, because it contains information about both pair and polyatomic distribution functions, and the position and shape of maxima do not correspond to interatomic distances and groups of atoms, owing to the effect of the backscattering amplitudes and phase shift. The values of the coordination numbers N_n, radii R_n of the coordination spheres, and the Debye–Waller factors σ_n^2 are derived as a result of simulation of the experimental EXAFS function. The problem of choosing the minimum number of components describing the signal is solved by applying the Nyquist criterion for the maximum number of parameters in the chosen windows in the k- and R spaces:

$$M_{\max} = (2\Delta k \Delta R)/\pi + 2. \quad (5)$$

For example, in simulation of the first coordination sphere of an $Al_{65}Cu_{22}Fe_{13}$ prephase crystal, Δk = 13.5 Å^{-1} and ΔR = 1.8 Å; therefore, the value $M_{\max} = 17$ obviously exceeds the number of parameters that is actually necessary for simulation. To refine the model used, it is desirable to use EXAFS spectroscopy in combination with X-ray or neutron diffraction. In this case, one can decrease the number of variable parameters, for example, fix the number of atoms in coordination spheres.

The Fisher criterion makes it possible to choose a model with the minimum number of parameters that adequately describes the experimental data. Let the numbers of parameters of the two models $\chi_1(k)$ and $\chi_2(k)$ be, respectively, M_1 and M_2 ($M_2 > M_1$). Then, the dispersions D_1 and D_2 can be written as

$$D_j = [M_{\max}/n(M_{\max} - M_j)] \sum_i [\chi(k_i) - \chi_j(k_i)]^2, \quad (6)$$
$$j = 1, 2; \quad i = 1 \ldots n$$

and, according to $F_{0.95\%}$ (Fisher criterion), the model $\chi_2(k)$ is accepted when $D_1/D_2 > F_{0.95\%}$. The values of $F_{0.95\%}$ are tabulated.

Samples

Bulk $Al_{65}Cu_{22}Fe_{13}$ samples were prepared by powder metallurgy using two techniques. In the first case, after mixing of powders of electrolytically pure metals, the charge was dried in air, and then pellets 10 mm in diameter and 2 mm in height were formed by cold pressing. These pellets were subjected to vacuum annealing at T = 800°C for two hours. In the second case, a prephase crystal was prepared in the first stage by vacuum thermal annealing at T = 500°C for 20 min. In the second stage, a quasicrystalline sample was

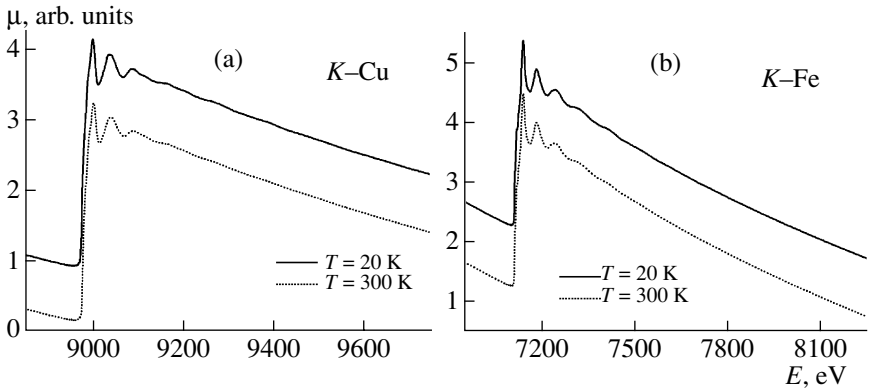

Fig. 2. EXAFS spectra of the i-$Al_{65}Cu_{22}Fe_{13}$ quasicrystal, measured at temperatures of 20 and 300 K above the (a) Cu and (b) Fe *K*-absorption edges.

obtained as a result of vacuum annealing at $T = 700°C$ for 20 min.

Furthermore, to prepare samples for measuring EXAFS spectra, the pellets were ground, carefully mixed with a cellulose powder to provide maximally homogeneous absorption over the sample thickness, and pressed into pellets 12 mm in diameter. The effective thickness x of the samples was chosen in accordance with the requirements for the optimal absorption jump $\mu x \approx 1.5$; the mass of each sample was about 15 mg, and the pellet area was 1.3 mm^2.

The X-ray diffraction analysis performed with a DRON-3 diffractometer and in the channel of the VEPP-3 storage ring at the Siberian Synchrotron Radiation Centre showed that no less than 95% of the prephase volume is occupied by the tetragonal ω phase (ω2213), whereas in the samples obtained by annealing and the two-stage process, no less than 90% of the volume is occupied by the quasicrystalline phase with an icosahedral structure (i2213). Investigations showed that the structure of the $Al_{65}Cu_{22}Fe_{13}$ prephase crystal corresponds with a good accuracy to the known structure of the analog crystal Al_7Cu_2Fe ($P4/mnc$).

RESULTS AND DISCUSSION

Figure 2 shows the typical EXAFS spectra of the ω2213 prephase crystal and the i2213 quasicrystal, measured at temperatures of 20 and 300 K above the *K*-absorption edges of (a) copper and (b) iron, respectively. Application of a special procedure for recording spectra, which makes it possible to increase the data collection time with an increase in the photoelectron wave vector $\sim k^2$, along with low-temperature measurements, provided a high signal-to-noise ratio up to $k \sim 16$ Å^{-1} (Figs. 3a, 4a). As a result, the reliability of the EXAFS data significantly increased in comparison with the previously published results [7, 8], which were obtained by analyzing shorter spectra (to ~12 Å^{-1}).

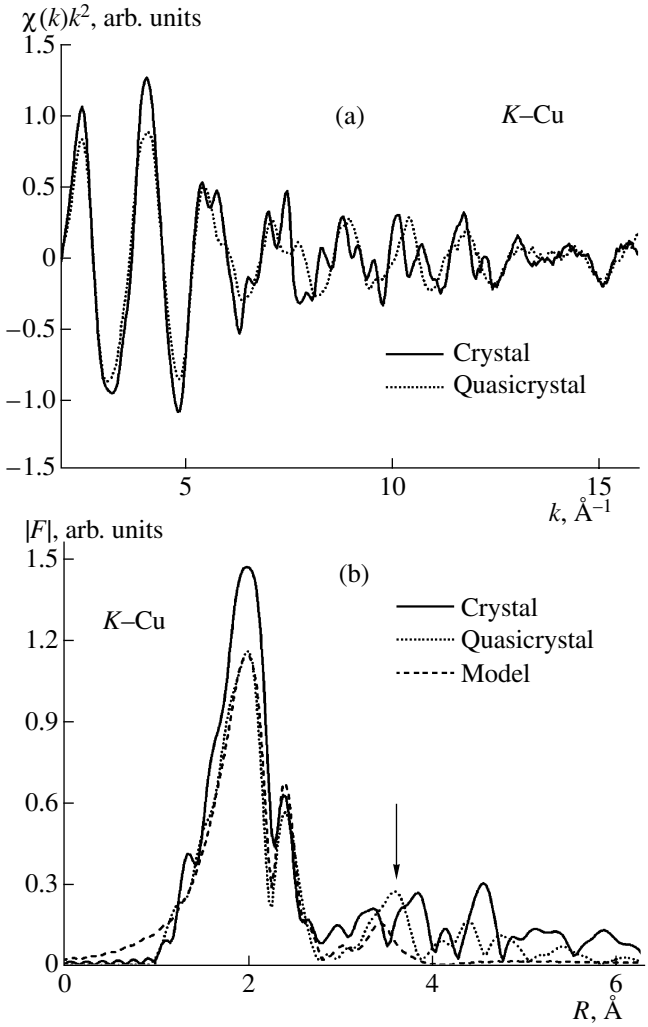

Fig. 3. (a) Experimental EXAFS function $\chi(k)k^2$, measured at $T = 20$ K above the Cu *K*-absorption edge and (b) the modulus of the Fourier transform $|F(R)|$ of the EXAFS function of the prephase crystal ω2213 and the i2213 quasicrystal.

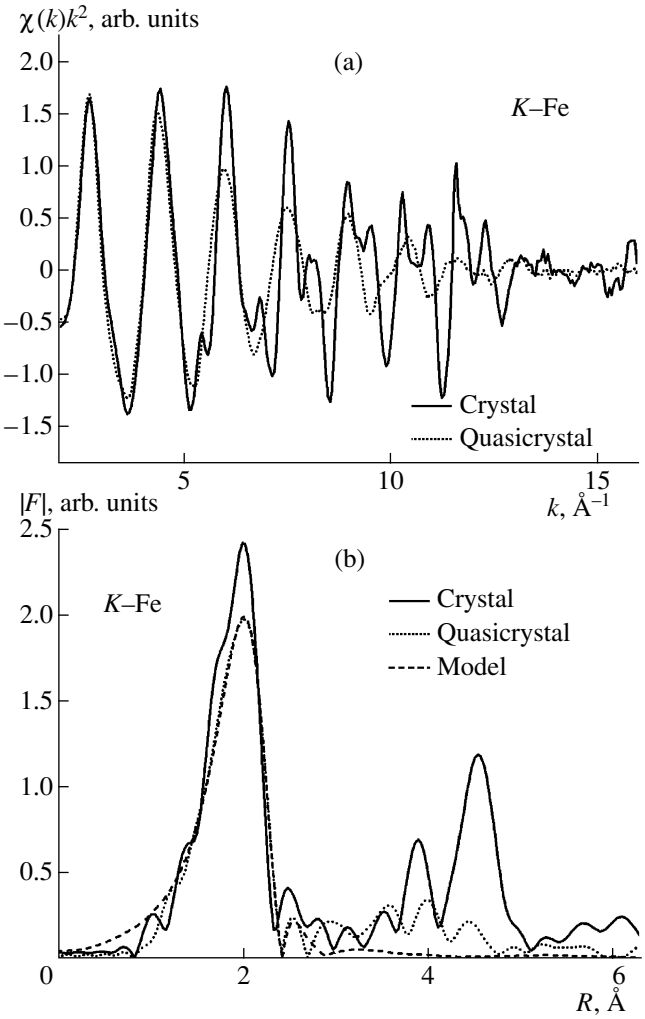

Fig. 4. (a) Experimental EXAFS function $\chi(k)k^2$, measured at $T = 20$ K above the Fe K-absorption edge and (b) the modulus of the Fourier transform $|F(R)|$ of the EXAFS function of the prephase crystal ω2213 and the i2213 quasicrystal.

The EXAFS functions and moduli of their Fourier transforms for the prephase crystal ω2213 and quasicrystal i2213 that were measured at 20 K and calculated above the K edges of copper and iron are shown in Figs. 3 and 4, respectively. Figure 3 indicates that not only the EXAFS functions of the crystal and quasicrystal that were measured above the Cu K edge but also the moduli of their Fourier transforms are in good agreement. The decrease in the amplitude of the maxima of $|F(R)|$ for the quasicrystalline sample in the range 1.0–2.8 Å is caused by some structural disordering of the nearest environment of copper. The differences in the farther region (to 3.5–4.1 Å) are more significant; however, the main features are repeated with some shift of the corresponding peaks to smaller distances in comparison with the peak position for the crystal. Analysis of the spectra showed that the local environment of copper in the quasicrystal is described fairly well by the model using the coordination parameters in the prephase crystal at fixed values of the coordination numbers and variation in the interatomic distances (see table). In this case, the best fitting of the model spectrum to the experimental one is obtained by replacing some part of Al(4) atoms with iron atoms. This model describes well not only the splitting of the first sphere but also the peak at a distance of 2.7 Å (Fig. 3b). At the same time, the peak indicated by an arrow near 3.7 Å is absent in the model spectra because it is due to the effects of multiple scattering. Thus, it follows from the EXAFS data analysis that the local structure around copper atoms is inherited by the quasicrystal from the crystal, with some shift and splitting of the nearest coordination spheres.

At the same time, the transition to the quasicrystalline state radically changes the structure of the local environment of iron. This change manifests itself, above all, in the significant decrease in the amplitude of the experimental EXAFS function (Fig. 4a). The modulus of the Fourier transform of the EXAFS function of the quasicrystal is more characteristic of amorphous systems (Fig. 4b). The shape and position of the peak $|F(R)|$ that corresponds to the nearest coordination sphere change, and the coordination spheres next to the nearest one (at distances of ~2.9 and ~4.5 Å) almost do not manifest themselves. This pattern indicates both rearrangement of atoms in the nearest sphere and the absence of particular ordering in the atomic arrangement beyond the nearest coordination sphere of iron in the quasicrystal.

Obviously, such significant changes cannot be described within the crystalline approximation, as in the analysis of the local environment of copper. As was shown in [10, 11], simulation of the experimental K-Fe EXAFS function gives the best results when the first coordination sphere around iron is an icosahedron. In contrast to the results of [7, 8], where the icosahedral environment was used also, it was demonstrated that the nearest sphere, along with aluminum atoms, includes copper atoms, which occupy positions of some aluminum atoms in the prephase crystal (table). As was noted above, in the nearest environment of copper in the quasicrystal, iron atoms with the coordination number $N \sim 0.5$ are found to be in the position of some aluminum atoms.

A similar result was recently obtained in [12] in the investigation of the EXAFS spectra of the α-$Al_{55}Si_7Cu_{25.5}Fe_{12.5}$ approximant. As can be seen in Fig. 5a, which was taken from [12], simulation of the first coordination sphere of iron requires the presence of heavy copper atoms along with light aluminum atoms. Otherwise, the model EXAFS function cannot be satisfactorily fitted to the experimental one. Concerning the nearest environment of copper (Fig. 5b), it contains both aluminum atoms and copper and iron atoms, as in the case of the $Al_{65}Cu_{22}Fe_{13}$

Parameters of the nearest environment of copper and iron in the crystalline and quasicrystalline $Al_{65}Cu_{22}Fe_{13}$ at $T = 20$ K (asterisks indicate the X-ray diffraction data of [9] for the analog Al_7Cu_2Fe crystal)

K edge	Crystal				Quasicrystal		
	type of atom	*N*	*R**, Å	R, Å	type of atom	*N*	*R*, Å
Cu	Al(1)	2	2.506	2.46	Al	2	2.47
	Al(2)	2	2.516	2.53	Al	2	2.52
	Cu(3)	2	2.610	2.59	Cu	2	2.64
	Al(4)	2	2.620	2.59	Al(Fe)	2	2.59
	Al(5)	2	2.710	2.69	Al	2	2.68
	Cu(6)	1	3.023	3.02	Cu	1	2.83
Fe	Al	1	2.447	2.33	Al	9	2.52
	Al	4	2.475	2.45	Cu	3	2.59
	Al	4	2.478	2.64			

quasicrystal (table). It can be seen in the figures reported that the contributions of light aluminum atoms and heavy copper and iron atoms to the EXAFS function corresponding to the first coordination sphere are in antiphase owing to the different photoelectron backscattering phase shifts.

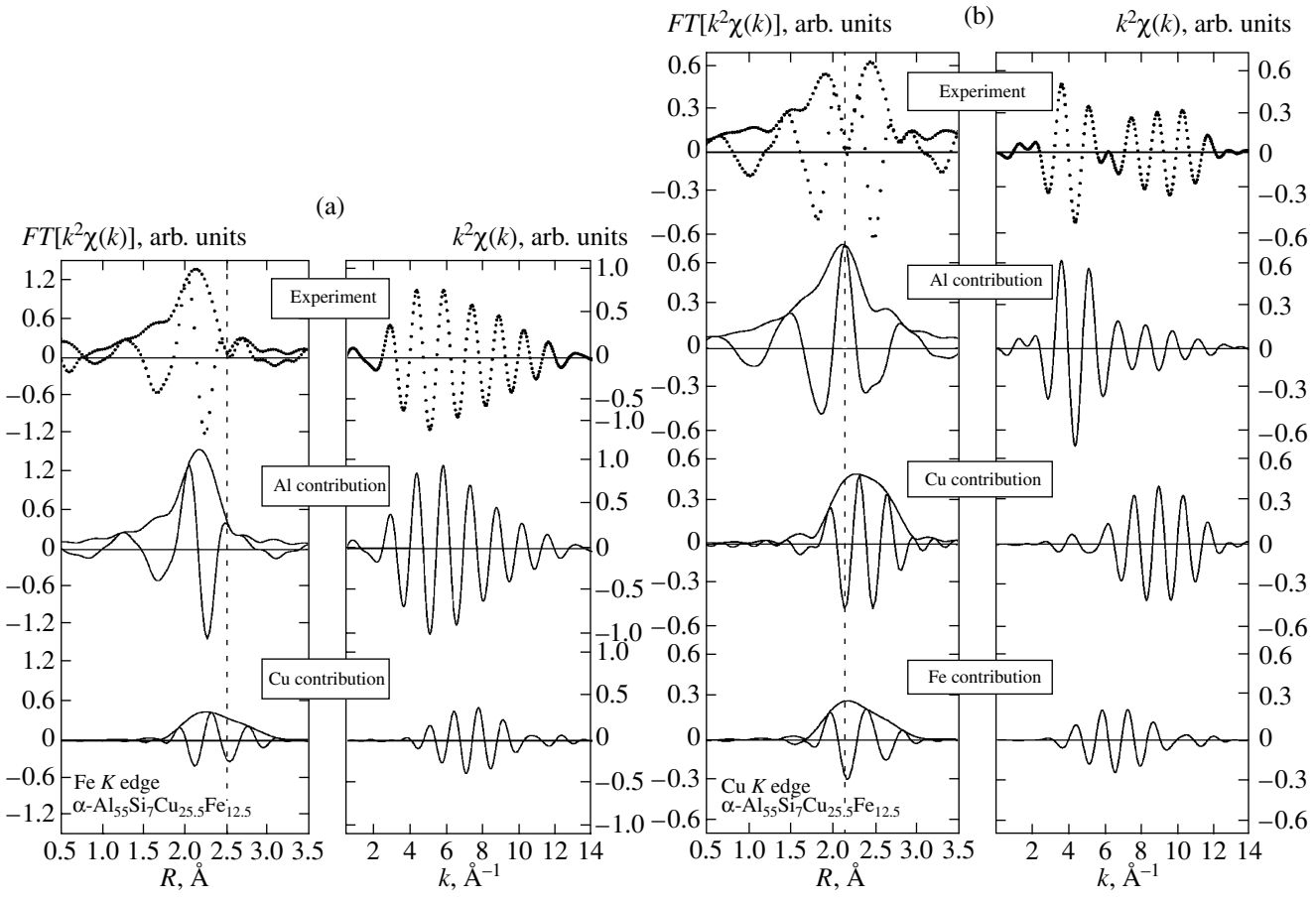

Fig. 5. Moduli of the Fourier transforms $|F(R)|$ of the EXAFS functions and the results of the inverse Fourier transformation corresponding to the first coordination sphere of the approximant of α-$Al_{55}Si_7Cu_{25.5}Fe_{12.5}$ for (a) Fe *K*- and (b) Cu *K*-absorption edges [12]. The vertical lines indicate the antiphase contributions of (a) Al and Cu and (b) Al and Cu(Fe).

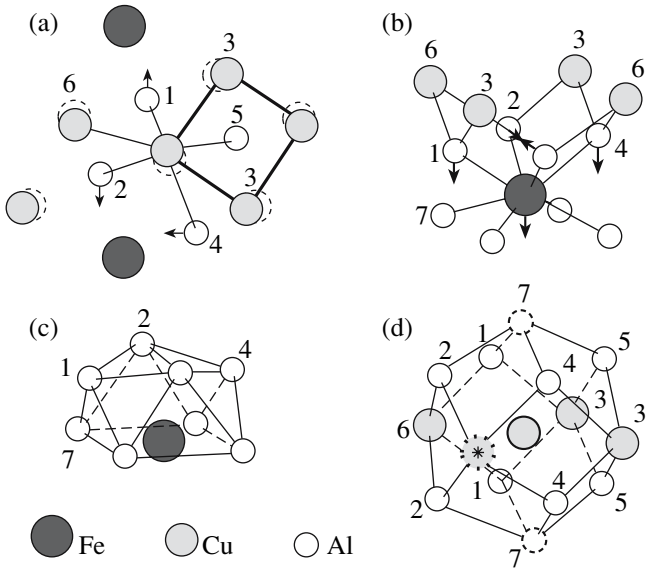

Fig. 6. Schematic diagram of the rearrangement of the local structure upon formation of a quasicrystal: (a) rotation of the copper subsystem (view along the *c* axis); (b) displacements of aluminum atoms, leading to the formation of an icosahedral cluster around iron atoms; (c) the top part of the icosahedron around iron; and (d) formation of a dodecahedron around copper. The asterisk indicates a vacancy in the environment of copper.

As a result of the joint EXAFS analysis of the features of the local environments of copper and iron, we proposed the following mechanism of local structural ordering of the quasicrystalline $Al_{65}Cu_{22}Fe_{13}$ phase. Upon transition from a crystal to a quasicrystal, the distance between the central copper atom and the copper atoms located in positions 3 slightly increases, whereas the increase in the distance to the copper atoms in positions 6 is much larger (Fig. 6a, table). With conservation (on the whole) of the symmetry of the local structure around copper atoms, the described change in the distances may be caused by the rotation of squares composed of copper atoms (with a simultaneous increase in the square side) toward the nearest aluminum atoms. Since the Cu–Al distance almost does not change upon the transition to the quasicrystalline phase, the aluminum atoms around copper shift, following copper atoms, with respect to iron to form an icosahedral cluster of pentagonal symmetry with an iron atom at the center (Figs. 6b, 6c).

The results of the investigation of the shape of the Cu and Fe *K*-absorption edges (the XANES spectra in Figs. 7a and 7b) are in favor of the mechanism proposed. It can be seen in Fig. 7a that the structure of the absorption edge of copper changes insignificantly upon the transition from crystal to quasicrystal. The largest changes are related to the increase in the amplitude of peak *B* and the decrease in the amplitude of the main peak *C*. Conservation of the energy positions of the main features of the spectra indicates similarity of the symmetry of the nearest environment of copper atoms in the crystal and quasicrystal.

The changes in the shape of the absorption edge of iron are more dramatic: along with the significant growth in the amplitude of peak *B*, energy shifts of peaks *A*, *C*, and *D* are observed, which are indicative of changes in the symmetry of the local environment of iron. Simulation of the XANES spectra was performed using the FEFF program [6], which is based on the ab initio calculation of absorption spectra. The problem of exact description of the shape of the absorption edge is beyond the scope of this study; we only tried to implement the possibility of choosing a local environment model that would most adequately describe the energy positions of the main spectral features at reasonable cluster sizes. In analysis of the shape of the Cu *K*-absorption edge of the quasicrystal, using different forms of clusters [13], the model with the first coordination sphere around copper atoms in the form of a dodecahedron was found to be the most adequate. The optimal simulation results are shown in Fig. 7a by a dotted line for a 5.23-Å cluster, which contains 57 atoms. An increase in the cluster size leads only to an increase in the time of count and does not significantly improve the simulation quality; this result is an additional confirmation of symmetry conservation and a high degree of ordering of the local environment of copper in the quasicrystal. The existence of several nonequivalent iron positions in the quasicrystal [14] hinders unambiguous simulation of the shape of the Fe *K*-absorption edge. The best model is the icosahedral one; the local character of ordering of the nearest environment of iron is confirmed by the fact that satisfactory results (Fig. 7b) are obtained only when sufficiently small (4.61 Å) 43-atom clusters are used. An increase in the cluster size led to deterioration of the simulation results, a fact indicating symmetry violation and confirming the conclusion of the EXAFS analysis about structural disorder beyond icosahedral clusters of the environment of iron.

Thus, joint analysis of the EXAFS and XANES spectra above the Cu and Fe *K*-absorption edges allows establishment of some characteristic features of changes in the local structure upon transition from the crystalline to the quasicrystalline state, which are schematically shown in Fig. 6.

In accordance with the results of the EXAFS analysis, rotation of copper squares causes rearrangement of aluminum atoms, which leads to the formation of icosahedral clusters around iron atoms. These changes are described in the form of phases (a) and (b) in Fig. 6. The top part of the icosahedral cluster surrounding an iron atom is shown in Fig. 6c, and Fig. 6d demonstrates the resulting cluster in the form of a dodecahedron around copper atoms, according to the XANES data. The positions of vertices 7 are close to Al positions in the crystal, and one of the sites in the plane saturated with copper is vacant. The vacancy is located at distances of ~2.5 and 4.0 Å from the nearest copper atoms. The presence of a vacancy in the nearest environment of copper in the quasicrystal is in complete correspon-

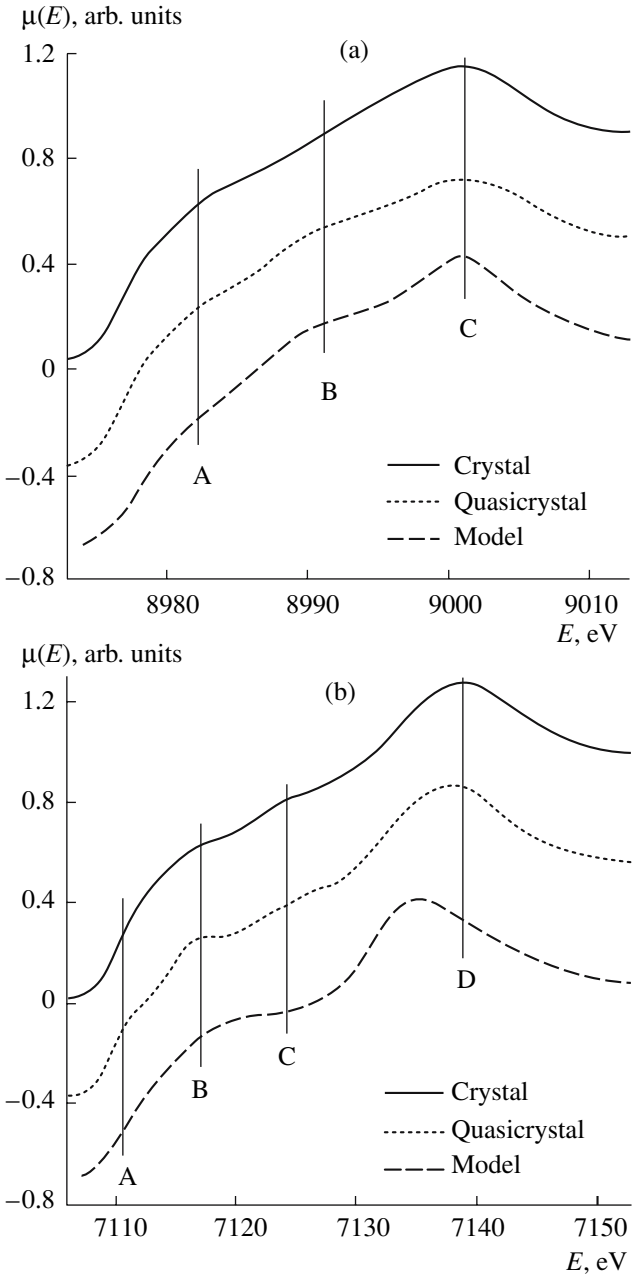

Fig. 7. (a) Cu and (b) Fe *K*-absorption edges for the prephase crystal ω2213 (solid line) and quasicrystal i2213 (dotted curve) at 20 K. The dashed line shows the result of simulation for the quasicrystal.

dence with the results of the quasi-elastic neutron scattering study, which revealed fast ($\tau \sim 160$ ps) local jumps of copper atoms at distances of ~2.5 and ~4.0 Å [15]. In the case under consideration, local jumps of iron atoms are much slower: $\tau \sim 160$ ps.

CONCLUSIONS

Thus, we have shown the main advantages of X-ray absorption spectroscopy for studying the local structural features of quasicrystals. On the basis of the observation of the local rearrangement of atoms upon the formation of an icosahedral structure in Al–Fe–Cu ternary alloys and by using a combination of EXAFS and XANES spectroscopy, we have proposed a model for the mechanism of structural crystal–quasicrystal transition. In summary, it should be noted that the mechanism considered here is in agreement with the conclusions about the important role of copper in the formation of electronic states on the Fermi surface in quasicrystalline Al–Cu–Fe [16]. On the basis of the X-ray photoemission study, it was shown in [16] that the Cu 3*d* states shift the densities of the Al 3*p* and Fe 3*d* states to higher and lower binding energies, respectively, thus facilitating the Fe3*d*-Al3*p* hybridization and total decrease in the density of states with the formation of a pseudogap on the Fermi surface.

ACKNOWLEDGMENTS

We are grateful to M.N. Mikheeva, A.A. Teplov, A.M. Bryazkalo, and G.V. Laskovaya for supplying samples and for useful discussions, the Program Committee of HASYLAB for the possibility of carrying out experiments on the synchrotron source, and K.V. Klement'ev for the help in carrying out the experiment. This study was supported by the Russian Foundation for Basic Research, project no. 05-02-16996-a.

REFERENCES

1. D. Shechtman, I. Blech, D. Gratias, and J. W. Cahn, Phys. Rev. Lett. **53**, 1951 (1984).
2. V. F. Gantmakher, Usp. Fiz. Nauk **172**, 1283 (2002).
3. J.-M. Dubois, Mater. Sci. Eng. **294–296**, 4 (2000).
4. K. V. Klementev, J. Phys. D: Appl. Phys. **34**, 209 (2001).
5. M. Newville, J. Synchrotron Radiat. **8**, 322 (2001).
6. A. L. Ankudinov, B. Ravel, J. J. Rehr, and S. D. Conradson, Phys. Rev. B: Condens. Matter Mater. Phys. **58**, 7565 (1998).
7. A. Sadoc, J. P. Itié, A. Polian, et al., Physica B **208–209**, 495 (1995).
8. J. P. Gomilšek, I. Arčon, A. Kodre, and J. Dolinšek, Solid State Commun. **123**, 527 (2002).
9. G. T. de Laissardière, Z. Dankahási, E. Bellin, et al., Phys. Rev. B: Condens. Matter Mater. Phys. **51**, 14 035 (1995).
10. A. P. Menushenkov, Ya. V. Rakshun, D. S. Shaĭtura, et al., Poverkhnost, No. 11, 66 (2003).
11. A. P. Menushenkov, Ya. V. Rakshun, M. N. Mikheeva, et al., Pis'ma Zh. Éksp. Teor. Fiz. **81**, 595 (2005) [JETP Lett. **81**, 479 (2005)].
12. V. Simonet, F. Hippert, R. A. Brand, et al., Phys. Rev. B: Condens. Matter Mater. Phys. **72**, 024 214 (2005).
13. K. Sugiyama, T. Kato, T. Ogawa, et al., J. Alloys Compd. **299**, 169 (2000).
14. P. P. Parshin, M. G. Zemlyanov, A. V. Mashkov, et al., Fiz. Tverd. Tela (St. Petersburg) **46**, 510 (2004) [Phys. Solid State **46**, 526 (2004)].
15. S. Lyonnard, G. Coddens, B. Hennion, and Y. Calvayrac, Physica B **234–236**, 28 (1997).
16. E. Belin, Z. Dankhazi, A. Sadoc, et al., J. Phys.: Condens. Matter **2**, 4459 (1992).

Translated by Yu. Sin'kov